DIAMOND

With Concentric Inclusions

As a diamond grows, layer by layer, it may incorporate small pieces of the surrounding mantle rocks as mineral inclusions. The three-dimensional arrangement of inclusions in most diamonds has the appearance of being somewhat random, with no discernible pattern. However, GIA's New York laboratory recently examined a noteworthy exception.

A 2.34 ct Fancy Intense yellow-green type IaAB diamond was found to have abundant silicate inclusions with a more systematic pattern delineating growth layers (figure 1). Collectively, the inclusions outline concentric octahedral layers. The growth layers are made even more noticeable by a sort of optical graining that could be caused by layered distortions in the diamond crystal from variations in nitrogen concentration. Many of the individual inclusions have an elongate or flattened oblate shape that conforms to the growth layering (figure 1, bottom). Thus, both the shape of individual inclusions and the collective distribution of multiple inclusions imitate the geometry of concentric octahedral diamond growth. This kind of symmetrical, growth-outlining texture is rarely observed in diamond.

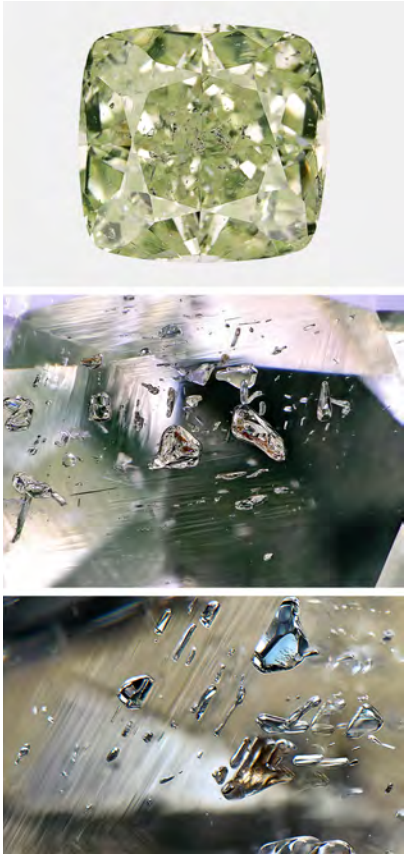

Figure 1. This 2.34 ct Fancy Intense yellow-green diamond (top) contains abundant inclusions that outline concentric octahedral growth layers. Through the table, the layers resemble nested rhombuses (middle, field of view 3.54 mm). The inclusion shapes appear to be controlled by the layering, as seen through the pavilion (bottom, field of view 1.99 mm).

The vibrant orange and green inclusions were identified as almandine-pyrope garnet and omphacitic clinopyroxene, respectively. Such mineral inclusions are distinctive of diamonds grown in an eclogite host rock, one of two common diamond rock types in the lithospheric mantle, the other being peridotite (S.B. Shirey and J.E. Shigley, "Recent advances in understanding the geology of diamonds," Winter 2013 *G&G*, pp. 188–222). Diamonds like this one with eclogitic inclusions are sometimes called E-type, while those with peridotitic inclusions are denoted as P-type.

This is an interesting sample from a geological perspective. There are still many unanswered questions about exactly how diamonds form. Detailed analysis of this sample could provide valuable clues as each layer captures successive chemical snapshots of the diamond growth process. Of particular interest here is the question of how long it takes to make a diamond. It is possible that this diamond grew over the span of millions of years and the inclusions serve as an encrypted record of the process.

Evan M. Smith and Wuyi Wang

With Unusual Fluorescence Distribution

The New York lab recently encountered a round brilliant diamond, weighing just over 2 ct, that displayed little if any reaction to long-wave UV except for a small spot confined to the area around the culet (figure 2, left). This small area appeared to have medium fluorescence intensity. While the laboratory determination of fluorescence strength and color is

Editors' note: All items were written by staff members of GIA laboratories.

Gems & Gemology, Vol. 53, No. 2, pp. 228–239.

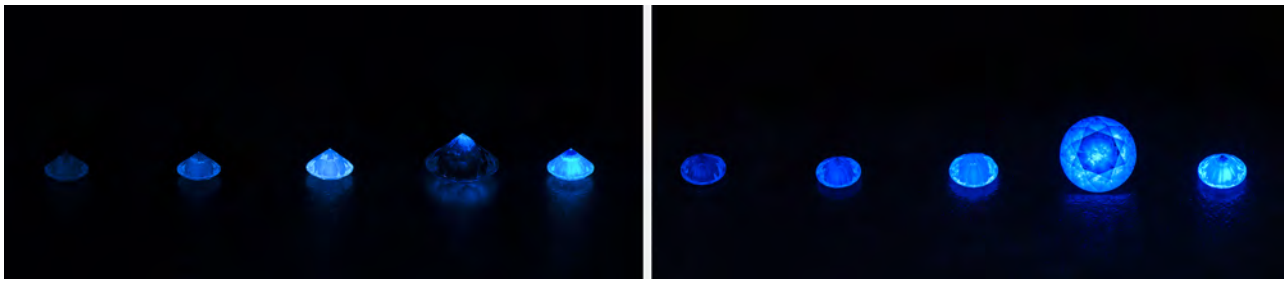

Figure 2. Left: The 2 ct round (second from right) displayed an unusual fluorescence reaction confined to the culet area. Right: When observed face-up, the small fluorescent area by the culet reflected throughout the stone and appeared more intense.

performed in the table-down position, we noticed a very different appearance when the diamond was observed through the crown (figure 2, right). Because of the location of the fluorescent area, it reflected evenly throughout the face-up position and appeared to have higher intensity, at approximately the strong/very strong boundary.

DiamondView imaging revealed that the diamond was cut with its growth zonation parallel to the girdle. We speculate that the area of fluorescence in the rough was larger and more centrally located, indicating that the earlier growth showed more blue fluorescence than the later growth, which was basically inert to UV radiation. With the given orientation and placement of the finished stone in the rough, a part of this fluorescent area remained at the culet in the cut stone, leading to this unusual feature.

Absorption spectra in the infrared region confirmed this to be a type Ia diamond with a high concentration of aggregated nitrogen and spectral features typical of a natural diamond. The N3 defect was detected by the presence of moderate-intensity absorption in the UV-Vis absorption spectrum, which is consistent with this type of diamond. The N3 defect is a well-known cause of blue fluorescence in natural diamonds. Based on past experience, it should be pointed out that the area at the culet with medium-strength blue fluorescence does not necessarily have higher concentrations of the N3 defect. The occurrence of other impurities or lattice distortion could affect fluorescence intensity from the N3 defect as well.

The effect of blue fluorescence on the appearance of D-to-Z diamonds has been debated for more than 25 years. GIA conducted a study on this subject in the 1990s (see T.M. Moses et al., "A contribution to understanding the effect of blue fluorescence on the appearance of diamonds," Winter 1997 *G&G*, pp. 244–259). The study showed that blue fluorescence had little to no impact on color appearance or transparency except in extremely rare examples of "overblues." With this in mind, the 2 ct round brilliant offered an interesting opportunity to revisit the earlier experiment's face-up observations. We compared the diamond, which was graded "H" color, with nonfluorescent diamonds—GIA color master stones—of similar color. As seen in figure 3, no visual difference was observed in the standard color-grading environment. This example supports the conclusion from the 1997 article that the industry would be better served by considering each diamond on its own visual merits.

John King and Wuyi Wang

Figure 3. No visible difference in color appearance or transparency was noted when the fluorescent stone was flanked by nonfluorescent diamonds of similar color in a color-grading environment.

Cat's-Eye KORNERUPINE

A dark, translucent, yellowish green oval cabochon (figure 4) was recently submitted to the New York lab for identification. The 1.44 ct stone displayed an intense chatoyancy.

With a spot refractive index (RI) reading of 1.67 and a hydrostatic specific gravity (SG) of 3.32, the stone was identified as kornerupine, a rare borosilicate mineral found in boron-rich volcanic and sedimentary rocks that have undergone metamorphism (http://rruff.info). Raman spectroscopy confirmed the identification.

Cat's-eye kornerupine is an extremely rare gemstone. Its chatoyancy

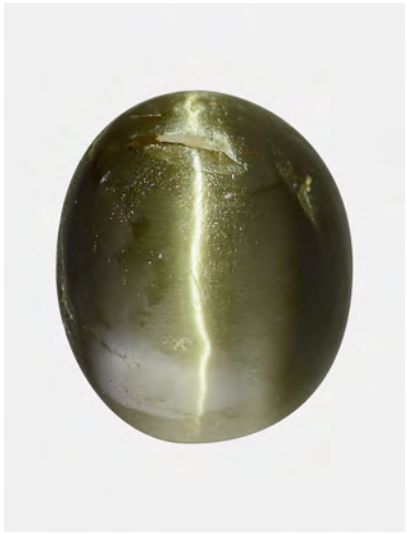

Figure 4. This 1.44 ct yellowish green kornerupine displayed strong chatoyancy.

is caused by rutile and graphite inclusions (H.N. Lazzarelli, *Gemstones Identification: Blue Chart*, 2010, www.gembluechart.com). However, we were unable to identify the needles in this stone using Raman spectroscopy. Fiber-optic illuminated magnification exposed dense clusters of these needles, some displaying iridescence (figure 5). This was GIA's first encounter with this material in more than a decade.

Akhil Sehgal and Daniel Girma

Figure 5. A dense collection of needle inclusions was the cause of the chatoyancy. Field of view 2.08 mm.

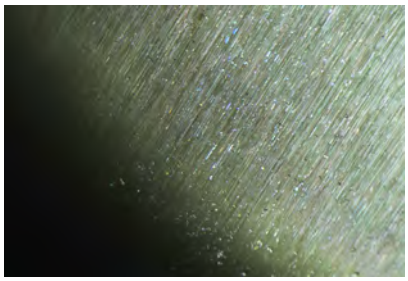

Natural Conch "Rosebud" PEARLS

Non-nacreous conch pearls from *Strombus gigas* are known mainly for their very attractive pink color and distinctive shimmering appeal due to the characteristic flame structures on their surfaces. Although conch pearls are found in various tones of yellow, brown, and white, the most desirable hue is undoubtedly pink with an intense saturation. The flame structures are due to "crosswise arrays of bundles of aragonite laths or fibers that may reflect or absorb the light that falls on the structure, letting it appear bright or dull" (H.A. Hänni, "Explaining the flame structure of non-nacreous pearls," *The Australian Gemmologist*, Vol. 24, No. 4, 2010, pp. 85–88).

In late 2016, GIA's New York lab staff had the opportunity to study part of Susan Hendrickson's conch pearl collection. Among the assortment of conch pearls of various sizes, colors, and shapes, a few "rosebud" specimens caught our attention (figure 6). The term "rosebud" is most commonly used to describe characteristically shaped freshwater nacreous pearls, but this is the first time GIA has examined conch pearls with such shapes (figure 7). The nine pink specimens had roundish outlines with a button-like appearance. But in keeping with the rosebud pearl form, they exhibited differences in the bumps or ridges on their surfaces. Some bumps were rounded and spread out, while others were jagged and tightly grouped. The authors could not locate any reports of rosebud conch pearls in the literature, and the cause of these distinctive surface structures is unknown. One possible explanation is that when a pearl forms in a pearl sac positioned in a region of muscular activity rather than the mantle, it will not form in a smooth symmetrical shape (E. Fritsch and E.B. Misiorowski, "The history and gemology of Queen conch 'pearls'," Winter 1987 *G&G*, pp. 208–221).

All nine samples displayed typical flame structures under magnification (figure 8). Some of them did not exhibit the flames on the bumpy surface, but only within the smoother areas. Microradiography revealed a tight internal structure with uneven outlines corresponding to the bumpy surfaces. The Raman spectra were characteristic of aragonite and clearly showed additional natural polyenic

Figure 6. "Rosebud" conch pearls of various pink tones ranging from 0.93 to 14.72 ct.

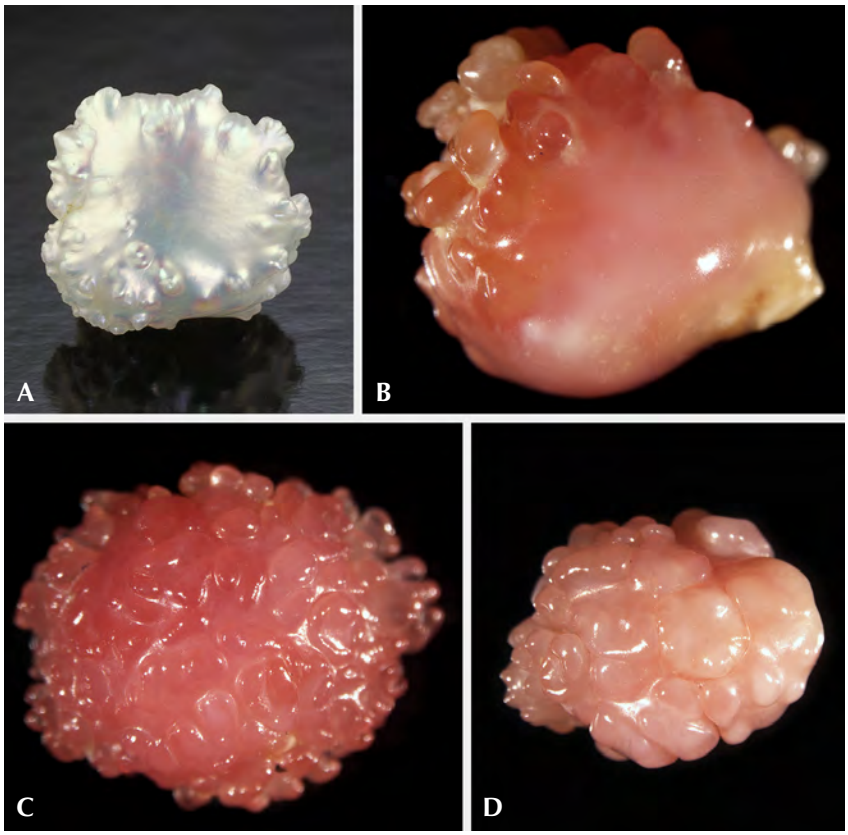

Figure 7. A shape comparison of a 4.90 ct American freshwater pearl exhibiting rosebud form (A) and three conch pearls, weighing 1.30, 0.66, and 0.91 ct (B–D).

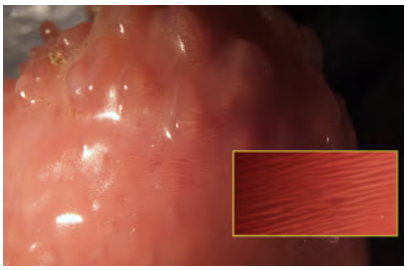

Figure 8. This 6.21 ct rosebud conch pearl shows characteristic flame structure at the surface. Fields of view 10.79 mm and 1.26 mm (inset).

pigment peaks, both as expected for pearls formed in *Strombus gigas* mollusks.

There are records of attempts to cultivate conch pearls (H. Acosta-Salmón and M. Davis, "Inducing relaxation in the queen conch *Strombus gigas* (L.) for cultured pearl production," *Aquaculture*, Vol. 262, No. 1, 2007, pp. 73–77; N. Sturman et al., "Cultured Queen conch pearls—A comparison to natural Queen conch pearls," 32nd *International Gemmological Conference*, Interlaken, Switzerland, 2011; Summer 2015 GNI, pp. 201–202). No further news about the commercial production of cultured conch pearls has reached the market, however. As a result, conch pearls are still highly desirable and valued by the trade and specialty collectors. The opportunity to study such unique and exciting examples of rosebud conch pearls allowed GIA to expand its understanding of rosebud conch pearls for future reference.

Joyce WingYan Ho and Emiko Yazawa

Partially Hollow Tridacna **Blister Pearls with Shells Attached**

GIA sees pearls of all types submitted to its global laboratories. Almost all of them are either loose or mounted in jewelry pieces; however, exceptions are occasionally encountered. The submission of a blister pearl or blister still attached to its shell is such an example (Winter 2015 Lab Notes, pp. 432–434). In January 2017, the Bangkok laboratory received an intact shell with a pearl attached near the adductor muscle area (figure 9, top). The item weighed 2.36 kg. The shell measured 32.0 × 21.0 × 11.5 cm, while the pearl measured 52.0 × 47.5 mm. At the same time and by sheer coincidence, another shell with a similar appearance and a pearl attached to the same area (figure 9, bottom) was submitted to the New York laboratory. This item weighed 806.40 g and the shell measured 20.0 × 13.5 × 9.5 cm, while the pearl measured 80.0 × 50.0 mm.

The exterior of the shell submitted to Bangkok exhibited a light brownish color and appeared roughly triangular in outline with a wavy pattern of thin ridges in rows, while the interior was white to cream with a porcelain-like surface. According to the client, the shell was found in 2014 by fishermen off the coast of Kood Island, a district of Trat Province in eastern Thailand. The shell's features are characteristic of *Tridacna* species mollusks, of which there are a number of varieties (U.E. Hernawan, "Taxonomy of Indonesian giant clams (Cardiidae, Tridacninae)," *Biodiversitas*, Vol. 13, No. 3, 2012, pp. 118–123).

As figure 9 (top right) shows, a blister pearl of similar color is prominently attached to the surface. Observation with a loupe and microscope confirmed that it was naturally attached and untreated. Microscopic examination using a fiber-optic light source confirmed the presence of flame structure on some surface areas

Figure 9. Two Tridacna *species shells with blister pearls in the adductor muscle area. Top: The shell of the specimen submitted to GIA's Bangkok lab weighs 2.36 kg and measures 32.0 × 21.0 × 11.5 cm. The blister pearl measures 52.0 × 47.5 mm (depth unmeasurable). Bottom: The shell of the New York sample weighs 806.40 g and measures 20.0 × 13.5 × 9.5 cm. The blister pearl measures 80.00 × 50.0 mm (depth unmeasurable).*

of the shell and pearl, confirming their non-nacreous or porcelaneous nature. The pearl's flame structure was short and patchy, while that seen on the shell was sharper and more defined. While the pearl's nomenclature may be the source of some debate, we considered it to be a blister pearl, rather than a blister, based on its external appearance, position on the shell, and size (E. Strack, *Pearls*, Ruhle-Diebener-Verlag, Stuttgart, Germany, 2006, pp. 115–127). The shell and pearl were exposed to long-wave UV, with the shell showing a moderate to strong chalky blue reaction with yellowish orange patches near the lip area (figure 10, left), while the blister pearl exhibited a weak to moderate yellowish green color (figure 10, right). This demonstrates how fluorescence in samples may vary from area to area.

However, the most noteworthy feature of the Bangkok specimen was that when the shell was tilted or gently rocked from side to side, a liquid clearly moved within the blister pearl (figure 11, left). The liquid was not viscous and so was most likely water, rather than a thicker liquid such as oil. It is possible that seawater was trapped during the blister pearl's formation or found its way into the "hollow" pearl at a later date. When fiber-optic light was used to illuminate the blister pearl, some of the light was transmitted and made the pearl appear translucent (figure 11, right). This, together with the trapped liquid, proved the pearl was at least partially hollow (see video at http://www.gia.edu/gems-gemology/tridacna-blister-pearls).

To see the extent of the Bangkok blister pearl's void, we examined its internal structure using a real-time X-ray (RTX) machine. Although it was only possible to examine the pearl in one orientation owing to its position and size, the blister pearl quickly revealed its partially hollow form (figure 12, left). The various shades of gray within the white near-oval feature (solid pearl surface) prove that the blister pearl's interior is full of organic matter and/or air since the X-rays passed through with very little obstruction. While hollow or partially hollow pearls—both nacreous and non-nacreous—are not new (N. Sturman, "Pearls with unpleasant odors," GIA Laboratory, Bangkok, 2009, www.giathai.net/pdf/Pearls_with_unpleasant_odours.pdf), this is the first one GIA has encountered with such visible trapped liquid. Although the solid shell attached to the pearl displayed similar gray shades, this coloring relates more to the sample's thickness than anything else. A few small rounded, darker gray patches are voids caused by parasites boring within the shell rather than by structures within the blister pearl.

Figure 10. Exposure to long-wave UV produced a moderate to strong chalky blue reaction with yellowish orange patches in the shell of the Bangkok specimen (left) and a weak to moderate uneven chalky yellowish green reaction in the attached blister pearl (right).

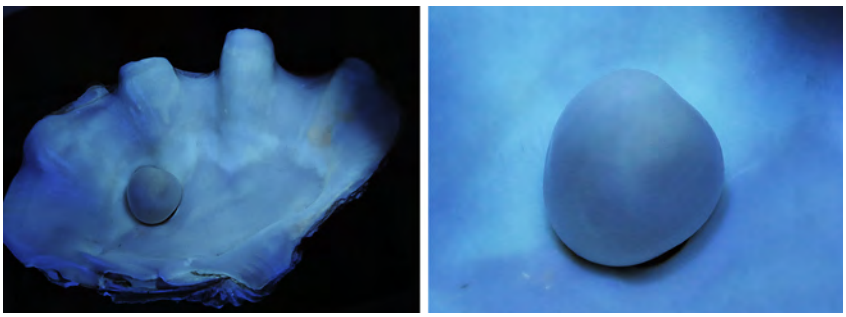

Figure 11. The blister pearl on the Bangkok submission shows a distinct boundary delineating the two phases (liquid and air) within the hollow pearl. The liquid part appears as a darker area and the air as a lighter area (left). Fiber-optic illumination reveals the boundary from a different perspective (right).

Void-like structures in whole or blister pearls from *Tridacna* species mollusks are not unusual (S. Singbamroong et al., "Microradiographic structures of natural non-nacreous pearls reportedly from *Tridacna* (clam) species," *Proceedings of the 5th GIT International Gem and Jewelry Conference*, Pattaya, Thailand, pp. 200–222), and GIA has examined many voids in other non-nacreous pearls. The RTX results proved that the specimen described was a natural blister pearl attached to its shell.

The shell submitted to GIA's New York laboratory is also noteworthy, not only for the coincidental submission, but also because the pearl was larger relative to its host's size than the one examined in Bangkok. The baroque natural blister pearl attached to this rather more colorful shell was also partially hollow, although not to the degree of the Bangkok sample. As the RTX results in figure 12 (right) revealed, the partially hollow blister pearl had a complex internal structure and was less homogenous than the specimen submitted in Bangkok. Unfortunately, no provenance was supplied with the New York sample, so there is no record of where it was found.

Both GIA reports stated that the naturally attached feature on each shell was a natural blister pearl. Many such specimens examined at GIA's labs are submitted as loose examples that have already been removed from their hosts, so it was a welcome change to handle these two shells. In addition, a comment was included on each report informing the clients of the pearl's partially hollow nature and, in the case of the Bangkok submission, the presence of a liquid. The size and appearance of the shells submitted proved they were not *Tridacna gigas* (giant clam), and the report referred to the hosts as *Tridacna* species only.

Nanthaporn Somsa-ard, Areeya Manustrong, and Joyce WingYan Ho

Figure 12. RTX results for the Bangkok sample (left) revealed a hollow pearl with a near-oval white ring marking the solid outline of the pearl's surface. Only parts of the New York pearl (right) were in the field of view at any one time due to its size. Neither appears to be entirely hollow; however, it was not possible to examine the pearls in other orientations due to their size and position on their hosts.

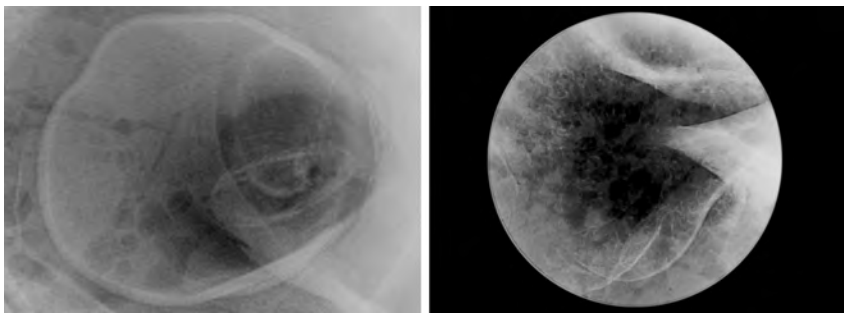

Atypical BEAD-CULTURED PEARLS With Unusual Nacre Growth

Atypical bead-cultured pearls are, by definition, cultured with unconventional beads as opposed to the typical round, predominantly freshwater shell beads. Examples of such atypical bead nuclei are irregularly shaped pieces of shell, ceramic, plastic, wax, coral beads, or even cultured or natural pearls.

Recently, GIA's New York laboratory received 10 loose undrilled pearls for identification. These samples exhibited a brownish bodycolor and measured from 7.17 × 6.92 × 6.42 mm to 12.25 × 9.72 × 9.28 mm (figure 13). Many were unusually lightweight for their size. Microradiographic examination of seven of the pearls revealed atypical bead nuclei (figure 14). The X-ray transparencies of the bead nuclei allowed us to observe faint demarcations and drill holes with varying degrees of clarity in the nuclei.

These atypical bead nuclei permitted some unusual nacre growth to develop within the drill holes, as shown in figure 14C, where the nacre secretion flows into the drill hole. This interesting observation concerning nacre viscosity was also described in recent work on atypical bead culturing experiments (K. Scarratt et al., "Atypical 'beading' in the production of cultured pearls from Australian *Pinctada maxima*," GIA Research & News, Feb. 13, 2017).

Figure 13. The 10 loose pearls submitted for identification. Samples 1, 4, and 5 are conventional bead-cultured pearls, while the rest were cultured with atypical nuclei. Photo courtesy of Aloha Pearls.

To better visualize the unusual nacre growth within the drill hole of the bead in one of the pearls, we used computed X-ray microtomography (μ-CT) and subsequently reconstructed the pearl using computer software (figure 15). The reconstructed image displayed a surface indentation aligned with the bead's drill hole (shown in orange in figure 15, left). Additional nacre growth (shown in green, figure 15, right) filled about half of the drill hole. The yellowish outer region in figure 15 (left) represents the outer nacre of the pearl.

Although this is not the first time GIA has received pearls cultured using X-ray transparent bead nuclei (Fall 2011 Lab Notes, pp. 229–230), the unusual nacre growth pattern within some of the drill holes in this sample group is worthy of note. Three-dimensional rendering using computer software and μ-CT data sets also proved very useful in visualizing the internal structure, further demonstrating the technique's worth as a powerful tool in pearl identification.

Chunhui Zhou and Emiko Yazawa

Punsiri Heat Treatment on Basalt-Related Blue SAPPHIRE

Heat treatment is often applied to sapphire to modify color or improve clarity. One known heat-treatment technique is the Punsiri method, typically applied to metamorphic or low-Fe blue sapphires. This treatment lightens the blue color by heating the stones in an oxidizing atmosphere to diffuse holes and aluminum vacancies into stones with low Ti levels (J.L. Emmett, lectures on corundum at GIA Bangkok, Aug. 28 and Dec. 4, 2010). The main characteristic of Punsiri heat treatment is distinct color zoning observable when the stone is immersed in methylene iodide. The stone will display a pale blue to near-colorless layer corresponding to the girdle outline that surrounds a deep blue core.

Recently, GIA's Bangkok laboratory examined a 1.63 ct blue sapphire, identified by standard gemological testing (RI of 1.760–1.769 and an inert reaction under long- and short-wave UV radiation). Microscopic observation revealed only a few inclusions, consisting of stringers and small healed fractures. We then immersed the stone in methylene iodide and observed Punsiri-type color zoning (figure 16). Fourier-transform infrared (FTIR) spectroscopy is a common technique used in advanced gemological laboratories to determine whether a stone is heated or unheated. When the FTIR spectrum shows Punsiri fea-

Figure 14. Microradiographs of seven pearls revealed atypical beads that were transparent to X-rays. The beads showed faint demarcations and drill holes of varying clarity. Unusual nacre growth that partially filled the drill hole of the bead of one pearl is seen in image C.

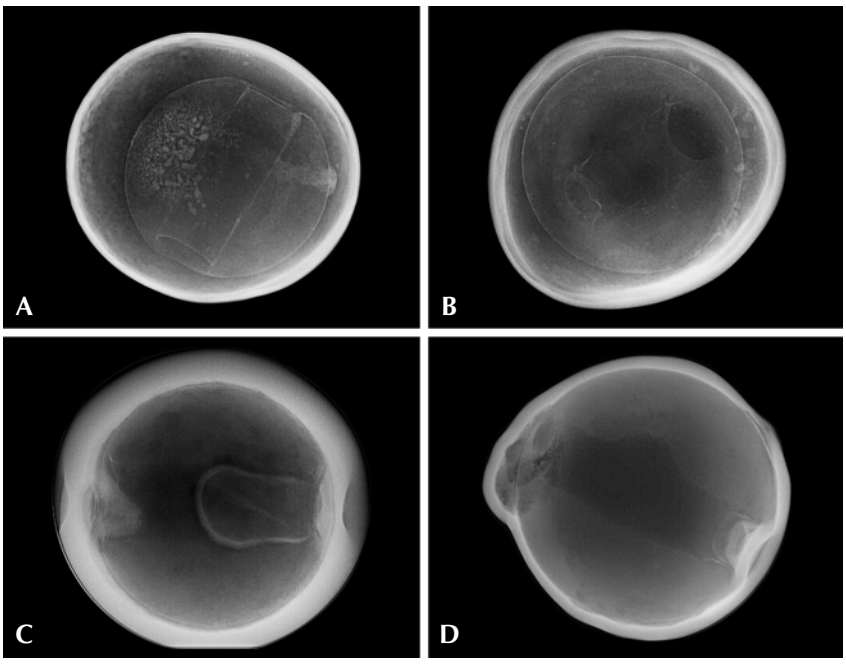

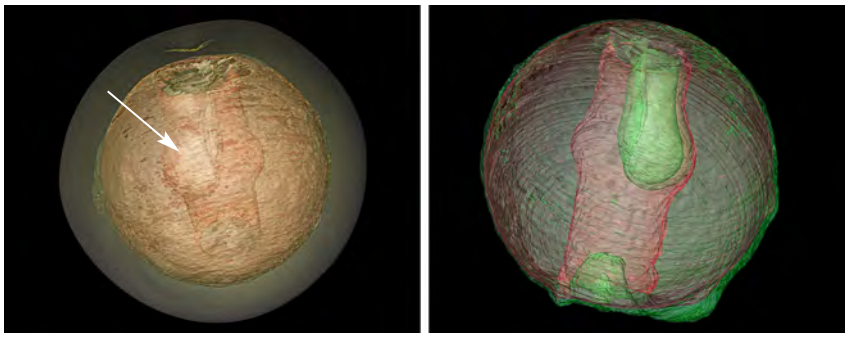

Figure 15. Left: A computed 3-D reconstruction of one of the atypical bead-cultured pearls. The orange area represents the transparent bead revealed by X-rays, with a drill hole partially filled by nacre growth shown by the whitish area (indicated by the arrow). A surface indentation toward the top also corresponds to the orientation of the bead's drill hole. Right: Reconstruction of the internal bead only. The central pink area is the drill hole inside the bead nucleus. The green area represents the nacre growth that formed inside the drill hole.

tures (e.g., multiband structures at 3191, 3064, 2626, and 2412 cm^{-1}; see chapter 4 of R.W. Hughes, *Ruby and Sapphire: A Gemologist's Guide*, RWH Publishing, Bangkok, 2017), this is conclusive for heat-treated metamorphic blue sapphire. However, when the FTIR spectrum does not show these features, it does not necessarily mean the stone has not been heat treated. Such was the case for this stone, which showed signs of heat treatment through its distinctive color zoning and near-colorless rim.

UV-visible near-infrared (UV-Vis-NIR) spectroscopy revealed a broad band at about 880 nm, indicating a blue sapphire of basalt-related origin. Laser ablation–inductively coupled plasma–mass spectrometry (LA-ICP-MS) showed no beryllium and limited amounts of other trace elements: 7 ppma Ti, 860 ppma Fe, and 47 ppma Ga were detected. This is the first time we have observed Punsiri heat treatment on a basalt-related blue sapphire. It was possible to perform the treatment on this sample due to the low amount of Ti, which allowed for faster diffusion. This report demonstrates the importance of the immersion technique in identifying heat treatment.

Sudarat Saeseaw

Figure 16. The 1.63 ct blue sapphire treated by the Punsiri method. Different views show a typical light blue to near-colorless outer layer when the stone is immersed in methylene iodide.

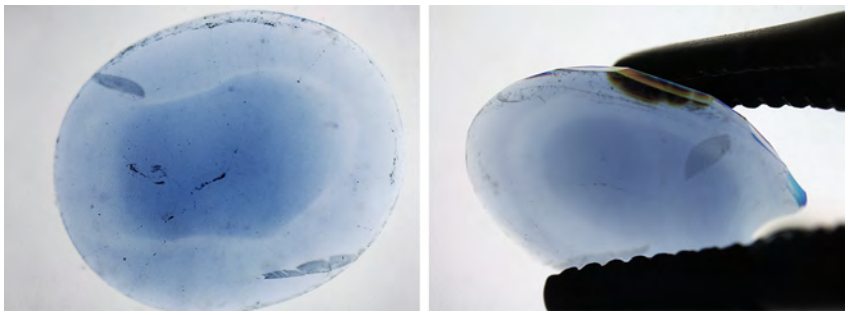

CVD SYNTHETIC DIAMOND Mimicking Natural Stone

A 0.51 ct round brilliant (figure 17) was recently submitted to GIA's Hong Kong laboratory for update service to verify the results from a diamond grading report issued in 2014. Investigation showed that its properties were much different from the diamond in the original report and that it was actually a CVD synthetic diamond.

The round brilliant submitted (5.18–5.20 × 3.11 mm) had H-equivalent color grade, much lower than the D color of the diamond submitted in 2014 (5.07–5.09 × 3.15 mm). Its IF-equivalent clarity was better than the VVS_1 clarity of the original stone, however. Only pinpoints and blemishes observable with greater than 10× magnification were found in this specimen. A GIA report number inscribed on the girdle was easily identified as a fake (figure 18). A minor difference in weight was also observed: an "increase" from 0.50335 ct to 0.51444 ct.

Infrared absorption spectroscopy identified the synthetic as type IIa and led to further spectroscopic testing. Photoluminescence (PL) spectroscopy was performed at liquid nitrogen temperature, and spectra

Figure 17. This 0.51 ct CVD synthetic diamond, submitted to GIA for update service, yielded some surprising results.

Figure 18. The GIA report number of a natural diamond graded three years earlier was inscribed on the CVD synthetic diamond shown in figure 17.

Figure 19. These 101 CVD synthetic diamonds were mixed into a parcel of 323 diamond melee, representing 31.3% of the stones.

were collected with various excitation wavelengths. A very strong SiV^- doublet observed at 736.6 and 736.9 nm indicated a synthetic diamond. Under the short-wave UV radiation of the DiamondView, the sample showed green fluorescence but, interestingly, none of the obvious layered growth structures that CVD synthetics usually display. All gemological and spectroscopic features confirmed that the stone was CVD synthetic with post-growth HPHT annealing. This is another example of the importance of using a combination of tests and data to identify a stone. GIA's laboratories continue to develop and implement various measures to identify possible fraud.

Billie Law

Melee Diamond Parcel Containing Nearly One-Third CVD Synthetics

In February 2017, a parcel containing 323 colorless to near-colorless diamond melee was submitted to the Mumbai laboratory for screening and color sorting. The average weight of each round brilliant was 0.015 ct, with an average diameter of 1.5 mm. Of this parcel, GIA's fully automated screening and sorting system confirmed that 219 samples were natural, with the remaining 104 samples referred for further testing. Detailed analysis determined that three of the referred stones were natural, and the remaining 101 stones (31.3%) were CVD synthetics (figure 19).

This result is especially remarkable due to the type of synthetic observed. While the undisclosed mixing of HPHT synthetic diamonds in melee has become a primary concern of the diamond trade, CVD synthetics have been very rare in this size group (Fall 2016 Lab Notes, p. 307). The synthetics were color graded using the GIA melee sorting device for research purposes. The majority of the CVD synthetics were G/H (74.3%) in color, though the D–F (20.8%) and I/J (4.9%) color ranges were also represented.

Further analysis was conducted on these synthetics using FTIR and PL spectroscopy (the latter at liquid nitrogen temperature) and DiamondView imaging. Interestingly, the group included both as-grown (10.9%) and treated synthetics (89.1%), indicating that they may have been produced by different laboratories. The treated diamonds showed evidence of annealing at high temperatures for color improvement, probably under HPHT conditions. FTIR revealed that they were all type IIa, with only two samples (1.9%) showing the CVD-specific NVH^0 absorption peak at 3123 cm^{-1}. Several impurity complexes common in CVD synthetic diamonds were detected by PL spectroscopy, including $NV^{0/-}$ (575 and 637 nm, 100%), the 596/597 nm center (4.0%), SiV^- (736/737 nm, 100%), the 883/884 nm Ni-related center (13.9%; see J.P. Goss et al., "The lattice location of Ni in diamond: A theoretical study," *Journal of Physics: Condensed Matter*, Vol. 16, No. 25, 2004, pp. 4567–4578), SiV^0 (946 nm, 29.7%), and H2 (986 nm, 17.8%). The presence of $SiV^{0/-}$ and the 596/597 nm center were particularly indicative of CVD origin, as $SiV^{0/-}$ centers are routinely found in CVD synthetics yet are comparatively rare in other diamond materials. The 596/597 nm center has been observed only in CVD synthetics.

DiamondView imaging further emphasized the variety of CVD synthetics included in this parcel. The fluorescence of the as-grown CVD synthetics ranged from orange to red to pink, as seen in figure 20 (top left), due to emissions from $NV^{0/-}$ centers. The other samples showed the typical blue–green fluorescence associated with high-temperature annealed CVD synthetics (figure 20, top right). In an unusual finding, layered structures suggesting abrupt changes in growth conditions—which may include stopping and restarting growth—were seen in 35.6% of the CVD synthetic melee. These abrupt changes resulted in alterations to the impurity uptakes of the material, producing the layered structures. Layer thicknesses varied

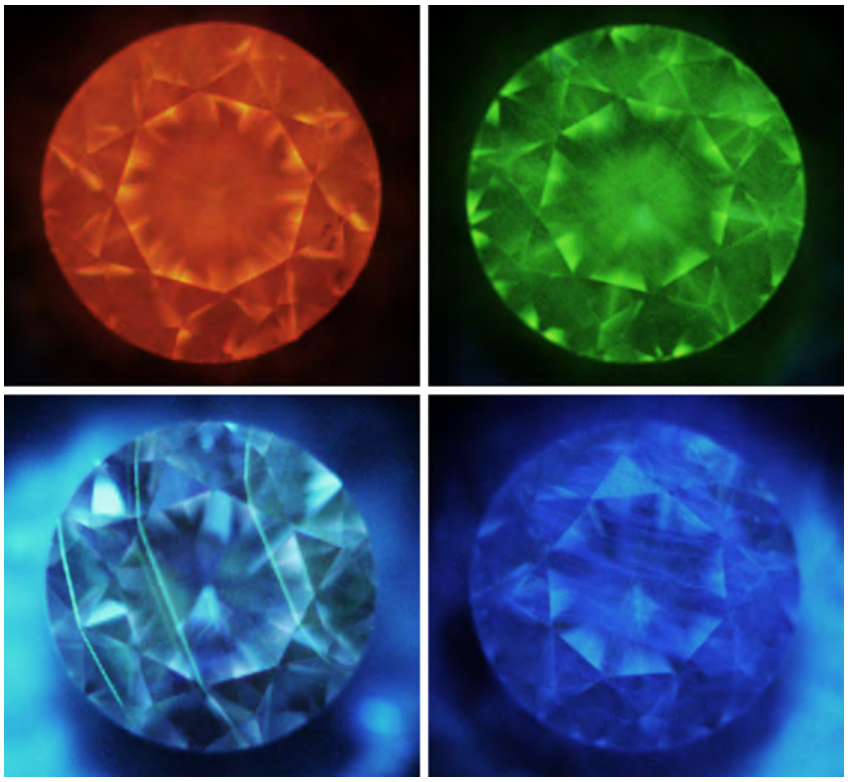

Figure 20. DiamondView images of the 101 CVD synthetic diamonds showed a wide range of patterns and colors, indicative of their different growth and treatment histories. As-grown synthetics showed orange, pink, or red fluorescence (top left), while those treated by high-temperature annealing fluoresced blue or green (top right). Slightly over a third (35.6%) of the synthetics showed layers indicative of changes in growth conditions (bottom left). Those with very high Si content were dominated by blue dislocation bundles (bottom right).

but were generally about 200–500 µm, with samples often showing two or more layers intersecting their table facets (figure 20, bottom left). Such layers are regularly seen in large CVD synthetics (Winter 2015 Lab Notes, pp. 437–439), though they have not been reported for melee-sized goods. Striations and blue dislocation bundles (the latter visible in figure 20, bottom right) were common (45.5% and 19.8%, respectively); certain high-Si synthetic diamonds were dominated by these bundles. Green or blue phosphorescence was observed for 84.2% of the CVD samples.

The substantial undisclosed mixing of CVD synthetic diamonds in this parcel, approaching one-third of the stones, emphasizes the importance of routine testing of melee to identify HPHT and CVD synthetics. GIA's automated melee screening and sorting device was able to successfully separate the natural and CVD synthetic material, providing confidence in the stones' origin and supporting transparency in the industry.

Manisha Bhoir, Priyanka Dhawale, and Ulrika D'Haenens-Johansson

CVD Synthetic Diamond Overgrowth on a Natural Diamond

Nitrogen is the most abundant defect in natural diamonds. It can be observed as single substitutional atoms or in aggregate forms. Boron, on the other hand, is a rare impurity in natural diamonds. It is very unusual to see both nitrogen and boron defects in a single diamond. GIA's New York laboratory recently encountered this in a 0.33 ct diamond graded Fancy blue (figure 21).

The infrared spectrum revealed something very unusual: a mixed type Ia and IIb diamond (figure 22). It also showed a platelet peak at 1367 cm^{-1} and a hydrogen peak at 3107 cm^{-1}. Mixed type Ia and IIb diamond occurs very rarely in nature; one was previously reported in *Gems & Gemology* (Spring 2009 Lab Notes, pp. 55–57). Nitrogen aggregation in this diamond was much higher, however. DiamondView images showed bluish green fluorescence in the face-up view and blue fluorescence in the face-down view (again, see figure 22). Detailed analysis using the DiamondView revealed a yellowish green fluorescence zone at the top of the crown with a sharp boundary in the crown facets (figure 22). PL spectra collected from the table and at the boundary in the crown facets showed emissions from SiV^- defects at 736.3 and 736.9 nm.

Although SiV^- defects can be observed in a natural diamond, the combination of SiV^- defects, a sharp boundary, yellowish green fluorescence, and phosphorescence sug-

Figure 21. This 0.33 ct Fancy blue diamond was confirmed to be a composite of CVD synthetic type IIb diamond overgrowth on a natural type Ia substrate.

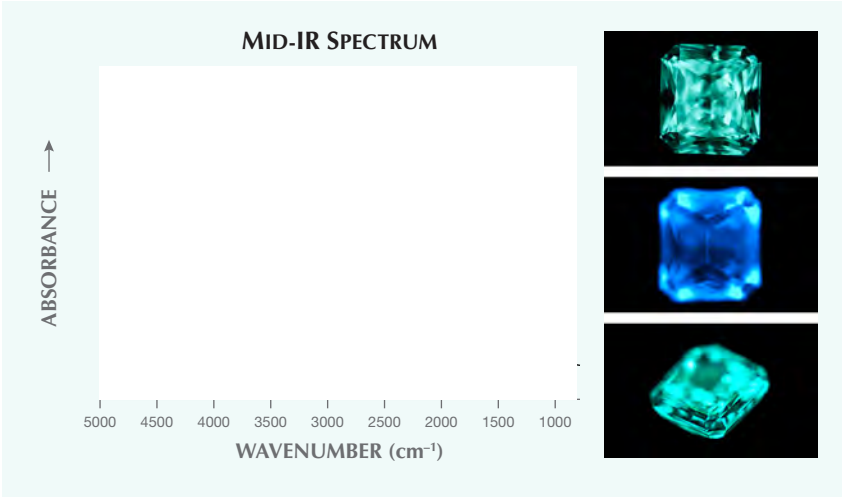

Figure 22. The mid-IR spectrum on the left revealed peaks for nitrogen aggregates and boron defects, along with a platelet peak at 1367 cm^{-1} and hydrogen peak at 3107 cm^{-1}. DiamondView imaging showed bluish green fluorescence in the face-up view (top right) and blue fluorescence in the face-down view (center right). The yellowish green fluorescent top layer was visible in a DiamondView image (bottom right).

gested that the top layer was CVD synthetic diamond. The bottom diamond showed blue fluorescence but no phosphorescence in the DiamondView, consistent with natural type Ia diamond. A distinct boundary line was observed along the interface layer on the crown facets (figure 23). The presence of the overgrowth layer was also clearly revealed through inspection with a variable pressure electron microscope set up to detect both secondary electron and panchromatic cathodoluminescence (CL) emission from the sample, providing topographical and compositional information (again, see figure 23). A distinct interface was visible through the pavilion in reflected light using a fiber-optic light source. A cloud-like inclusion, trapped at the interface layer, was also observed, as well as a dark needle located at or near the interface (figure 23). A small stress halo and a natural surface could be observed in the bottom diamond. The strain pattern throughout the pavilion was consistent with natural type Ia diamond.

The quality of a CVD synthetic depends on the crystallographic orientation and temperature of the seed crystal or substrate during growth. CVD synthetic diamond films have been grown on natural diamond substrates since the early 1960s (W.G. Eversole, U.S. patents 3030187 and 3030188, 1962). Methane and other carbon-containing gases were used, but graphite was deposited along with the CVD synthetic layers. In 1993, CVD synthetic layers were successfully grown on natural type IIa and Ia diamond substrates (see B.G. Yacobi et al., "Preferential incorporation of defects in monocrystalline diamond films," *Diamond and Related Materials*, Vol. 2, No. 2–4, 1993, pp. 92–99). They applied a mixture of CH_4 and H_2 at 80 torr in a microwave plasma-assisted CVD system. Reaction between CH_4 and H_2 produced H atoms, which maintained an sp3-bonded surface and prevented graphitization. The temperature applied to the natural diamond substrate during the CVD growth process of the sample we studied was relatively low, as suggested by the absence of single substitutional nitrogen atoms (N_s^0). It is also in agreement with Yacobi (1993), who applied temperatures of 880°C for CVD growth on type Ia {100} diamond substrates and 1200°C for type Ia {111} diamond substrates. Deposition of a boron-doped CVD synthetic film of <10 microns on a natural gem-quality diamond was reported in 2005 (Summer 2014 Lab Notes, p. 152); however, spectro-

Figure 23. Left: A distinct boundary line indicating an interface (marked with arrows) was seen under the microscope. A dark needle inclusion is located at or near the interface (near the center of the image). Field of view 1.95 mm. Center: An electron microscope image combining secondary electron and cathodoluminescence emissions reveals the presence of an overgrowth layer. Right: The CVD synthetic layer is approximately 80 microns thick.

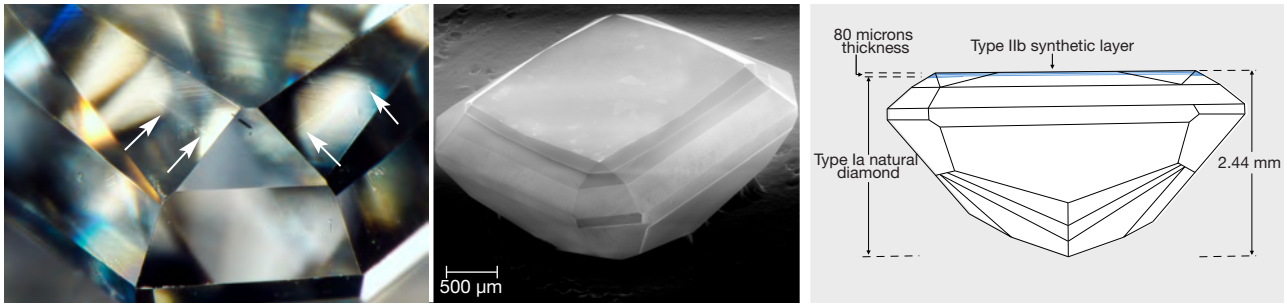

scopic analysis did not show boron and SiV^- defects.

Based on the growth pattern of the natural diamond, it is clear that the type IIb CVD diamond was produced in or very close to {100} orientation. The natural diamond substrate showed no observable inclusions except for a very small stress halo. The thickness of the CVD overgrowth layer was approximately 80 microns (again, see figure 23). FTIR spectroscopy is a bulk analysis, making it very hard to measure and separate IR spectra between a thin CVD layer on top and a thick diamond substrate. However, the fluorescence and phosphorescence reactions suggest that the top synthetic layer contained boron (e.g., boron-doped CVD synthetic) and the bottom diamond contained nitrogen aggregates. The thin layer of type IIb CVD synthetic diamond on the top of this stone effectively introduced Fancy blue color when viewed from its table.

This synthetic overgrowth on a natural diamond with a Fancy color grade is the first GIA has seen. Identification of colored diamonds should be performed very carefully by looking for unusual characteristics, such as a straight boundary line associated with an interface plane, and fluorescence zones with sharp edges in DiamondView images. Examination of this fancy-color composite diamond indicated that similar challenges could exist for colorless and near-colorless diamonds.

Kyaw Soe Moe, Paul Johnson, Ulrika D'Haenens-Johansson, and Wuyi Wang

Figure 24. Among the 70 melee diamonds mounted in this ring, one was confirmed to be an HPHT synthetic diamond.

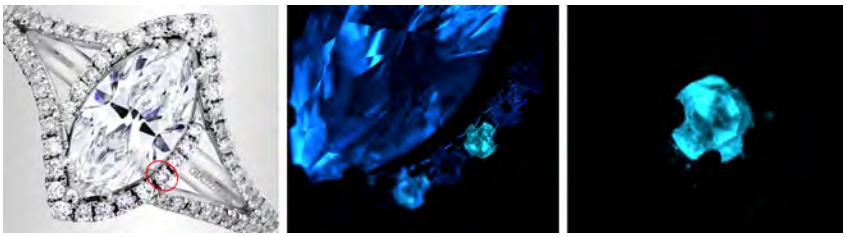

Figure 25. Set near the center marquise diamond, one melee diamond (left, in red circle) showed the blue fluorescence (center) and phosphorescence (right) characteristic of HPHT synthetic diamond.

HPHT SYNTHETIC DIAMOND
Melee Found in Mounted Jewelry

Separation of treated and synthetic diamond melee from natural diamond is challenging work. Diamond melee, which weigh less than 0.2 ct, are often submitted to gemological laboratories in parcels containing hundreds (or more) loose stones. GIA's automatic screening device, introduced in 2016, can separate synthetic and treated diamond melee from natural diamond melee. Identification becomes more challenging when the melee are mounted, due to their small size and the difficulty of accessing them.

In late February 2017, GIA's Hong Kong laboratory received a ring containing 70 melee in addition to a marquise-cut diamond center stone (figure 24). Using a prototype of GIA's new screening device for mounted gems, 69 of the melee passed the test for natural diamond, and one was referred as possible treated or synthetic diamond. The stone in question, which was set next to the center marquise diamond (figure 25, left), had no apparent inclusions. Infrared absorption spectroscopy identified it as a type IIb diamond with an absorption band at 2800 cm^{-1}, indicating the presence of boron as a defect, forming a local vibration mode. Using PL spectroscopy, a very strong doublet peak at 882/884 nm related to nickel impurity was recorded under laser excitation and low temperature. The NV^- center was more prominent than the NV^0 center. Strong blue phosphorescence was also detected (figure 25). These observations confirmed that this was an HPHT synthetic diamond, very similar to melee we have previously tested that were manufactured in China.

How to screen jewelry items with mounted diamonds for quality control is a concern in the industry. GIA's robust instrument for rapid and accurate screening of small diamonds set in mountings will be available in late 2017.

Terry Poon and Wuyi Wang

PHOTO CREDITS
Evan Smith—1; Jian Xin (Jae) Liao—2 and 3; Sood Oil (Judy) Chia—4, 6, 13, and 21; Daniel Girma—5; Tino Hammid—7 (top left); Joyce WingYan Ho—7, 8, and 9 (bottom); Nuttapol Kitdee—9 (top); Promlikit Kessrapong—10; Kwanreun Lawanwong—10; Emiko Yazawa—15; Sudarat Saeseaw—16; Johnny Leung—17, 24, and 25 (left); Tony Leung—17; Billie Law—18; Roxane Bhot—19; Priyanka Dhawale—20; Jemini Naik—20; Kyaw Soe Moe—22 and 23 (left); Ulrika D'Haenens-Johansson—23 (center); Terry Poon—25 (center and right).